This is an *Accepted Manuscript*, which has been through the Royal Society of Chemistry peer review process and has been accepted for publication.

Accepted Manuscripts are published online shortly after acceptance, before technical editing, formatting and proof reading. Using this free service, authors can make their results available to the community, in citable form, before we publish the edited article. We will replace this *Accepted Manuscript* with the edited and formatted *Advance Article* as soon as it is available.

You can find more information about *Accepted Manuscripts* in the **Information for Authors**.

Please note that technical editing may introduce minor changes to the text and/or graphics, which may alter content. The journal's standard **Terms & Conditions** and the **Ethical guidelines** still apply. In no event shall the Royal Society of Chemistry be held responsible for any errors or omissions in this *Accepted Manuscript* or any consequences arising from the use of any information it contains.

Journal Name

ARTICLE

Emerging Cool White Light Emission from Dy³⁺ doped Single Phase Alkaline Earth Niobate Phosphors for Indoor Lighting Applications

Amit K. Vishwakarma,[a] Kaushal Jha,[a] M. Jayasimhadri,*[,a] B. Sivaiah,[a,b] Bhasker Gahtori,[a,b] D. Haranath[b]

Single-phase cool white-light emitting $BaNb_2O_6$:Dy^{3+} phosphors have been synthesized via conventional solid-state reaction method and characterized using X-ray diffraction (XRD), scanning electron microscopy (SEM) observations and spectrofluorophotometric measurements. XRD and Rietveld strucutral refinement studies confirms that all the samples exhibit pure orthorhombic [space group- $C222_1(20)$]. SEM observations reveals the dense particle packaging with irregular morphology in micron range. The as-prepared phosphors exhibit blue (482 nm) and yellow (574 nm) emissions under 349, 364, 386 and 399 nm excitations corresponding to $^4F_{9/2} \rightarrow {}^6H_J$ (J= 15/2, 13/2) transitions of Dy^{3+} ions. The energy transfer mechanism between Dy^{3+} ions has been studied in detail and the luminescence decay lifetime for $^4F_{9/2}$ level was found to be around 146.07 μs for the optimized phosphor composition. The calculated Commission Internationale de L'Eclairage (CIE) chromaticity coordinates for the optimized phosphor is (x=0.322, y=0.339), which is close to the National Television Standard Committee (NTSC) (x=0.310, y=0.316) coordinates. The values of CIE chromaticity coordinates and correlated color temperature (CCT) of 5907 K endorses cool white-light emission from the phosphor. The study reveals that $BaNb_2O_6$:Dy^{3+} phosphor could be a potential candidate for near ultra-violet (NUV) excited white-LEDs applications.

1. Introduction

In recent years, rare earth ion doped inorganic luminescent materials have been extensively studied in the fields of materials science, physics, chemistry and life sciences due to various potential applications in display devices (e.g., cathode ray tubes, vacuum fluorescent displays, and field emission display), lighting gadgets (e.g., fluorescent tubes and white-light emitting diodes), solid-state lasers, biological labelling, X-ray, medical devices, ionization radiation and so on.[1-2] Among them, white light emitting diodes (w-LEDs) have been considered to be the next generation illumination sources in the field of solid-state lighting instead of traditional incandescent and currently implemented fluorescent lamps due to their numerous advantages such as small size, high energy efficiency, energy-saving, robustness, high brightness, fast switching, longer life time (>100 000 h) and environmental friendliness.[3-5] Currently, two approaches have been implementing to achieve white light through solid-state lighting (SSL). The first one is phosphor-free SSL approach employing RGB-LEDs, which consist of red, green and blue monochromatic LEDs to obtain white-light. The main drawback of this approach is that every LED must be adjusted by individual power supply to balance the emission intensity of each color. However, the second approach involves phosphor integrated to the SSL device. The phosphor-converted (pc) LED uses an ultra-violet (UV)/near ultra-violet (NUV) light in combination with single/multiple phosphors that convert a part of the light emitted by the UV/NUV LED into white-light.[6,7] At present, most of the commercially available w-LEDs are based on the second approach because of the simplicity in operation. The combination of blue LED (InGaN) coated with yellow-emitting ($Y_3Al_5O_{12}$: Ce^{3+}) phosphor is one of the widely used approach currently to produce w-LEDs. However, this approach encounters some serious issues such as halo effect of blue/yellow color separation, color dependence on chromaticity, and poor color-rendering index (<65) due to the lack of green and red-emitting phosphor components at long wavelength region, which limits the LED applications further.[8] On the other hand, UV/NUV LED coated with multicolor-emitting phosphors is an alternative approach to obtain white-light emission with an excellent color-rendering index (>90) as the luminous efficiency of NUV/UV chip pumped w-LEDs is higher than the blue chip[9]. However, UV/NUV excitable multiple color-emitting phosphors have some disadvantages such as low luminous efficiency due to blending together of blue, green and red-emitting phosphors and different degradation schedules of each phosphor.[9,10] Therefore, single phase phosphor has become a necessary pre-requisite for the fabrication of w-LEDs using UV/NUV LED chips to overcome the problems mentioned above. There are different methodologies to obtain white light emission from single phase host lattice by (i) doping single rare earth (RE) ion, (ii) doping of two or more RE ions, which are excited simultaneously, (iii) co-doping of different ions and controlling the emission via energy transfer processes, and (iv) controlling the concentration of the defect and reaction conditions of defect related luminescent materials.[11]

Alkaline earth niobates have emerged as novel materials with huge technological and scientific importance due to their excellent non-linear optical, photocatalytic, piezoelectric, ionic

a. *Luminescent Materials Research Lab, Department of Applied Physics, Delhi Technological University, Delhi 110 042, India*
b. *CSIR-National Physical Laboratory, Dr. K.S. Krishnan Road, New Delhi 110 012, India*

conductive and photorefractive properties for the applications involving acoustic transducers, delay lines in filters, optical modulators, beam deflectors etc.[12,13] Among all inorganic phosphors, oxide based phosphors are preferred choice for display and SSL applications due to their exceptional chemical stability, inertness and moisture resistance. Moreover, rare-earth doped alkaline earth niobate phosphors have attracted much attention and have been applied for light emitting diodes (LEDs) and plasma display panel (PDP) applications.[14] The metaniobate ceramic, with the general formula $M^{2+}Nb_2O_6$ (M^{2+}=divalent alkaline earth or transition metals) are sub-component of the complex perovskite family, $A(M_{1/3}Nb_{2/3})O_3$ and they are mostly exist in an isostructural form of orthorhombic structure with columbite mineral group with the exception of the M=Sr, Ba and Pb analogues, which crystallize in different orthorhombic structures.[15-17] In this quest, barium metaniobate ($BaNb_2O_6$) has been selected as host lattice due to its smaller band gap and exhibits higher charge generation under UV light irradiation compared to other binary niobates. Moreover, $BaNb_2O_6$ has been widely used as a high quality refractory material for photocatalytic and microwave dielectric applications in recent years.[18] The luminescent properties of various rare-earth ions doped niobate phosphors have been investigated and reported elsewhere.[19-21,14] However, to the best of our knowledge, luminescent properties of Dy^{3+} ions doped $BaNb_2O_6$ phosphors has never been reported in the literature. Hence, in the current study, the said phosphor has been chosen to synthesize and investigate thoroughly for the first time. In addition, it is well-known that Dy^{3+} ions with $4f^9$ electronic configuration has complex energy levels and various possible transitions between f-f levels that are highly selective and exhibit sharp line spectra.[22] It gives emission in blue and yellow band and the intensity ratio of these two emission bands depends on the host crystal structure.[23,24]

In the current work, a series of Dy^{3+} ions doped single-phase $BaNb_2O_6$ phosphors have been prepared by solid-state reaction method to explore its possibility as potential phosphor for white-LEDs by investigating photoluminescence and colorimetric properties in detail.

2. Experimental procedure

$Ba_{(1-x)}Nb_2O_6$:xDy^{3+} (where x = 0.01, 0.1, 0.5, 1.0, 1.5, 2.0 and 2.5 mol %) were synthesized by conventional solid-state reaction method. The precursor chemicals namely, $BaCO_3$ (Fisher scientific, 99%), Nb_2O_5 (Fisher scientific, 99.9%) and Dy_2O_3 (Sigma Aldrich, 99.9%) all of AR grade were taken as starting materials. A stoichiometric amount of precursor materials were thoroughly mixed using an agate mortar and pestle for an hour with acetone as dispersing medium. Raw powder sample was kept in an alumina crucible and then heated in a programmable muffle furnace at 625^oC for an hour to remove CO_2 and then sintered at 1200^oC at heating rate 6 ^oC min^{-1} for 5 hour in air atmosphere. Finally, the sample was naturally cooled to room temperature (~25^oC) in the furnace itself.

The structure of the prepared sample was determined through XRD. The crystalline phases were identified by X-ray diffractometer (Rigaku make, model-Mini flex-II), using nickel-filtered Cu K_{α} radiation (λ= 1.54056 Å) in the range of 20°≤ 2θ ≤ 60° and the accelerating voltage was kept at 30.0 kV and tube current at 15 mA. The FullProf suite programme was used to reveal the structural refinement. The morphological observations were carried

out by SEM (Hitachi, Model- S-3700N). The photoluminescence excitation (PLE) and photoluminescence (PL) spectra were recorded using Shimadzu spectrofluorophotometer (model: RF-5301PC) fitted with a Xenon flash lamp. The lifetime measurement was carried out using a time-resolved luminescence spectrometer (model- F900 Edinburgh), equipped with a time correlated single photon counting system and microsecond xenon flash lamp as the source of excitation.

3. Colorimetric theory

The color of any object (self luminous or reflecting) can be conveniently specified via Commission International de L' Eclairage (CIE) chromaticity coordinates marked on a chromaticity diagram.[25] These color coordinates are calculated from the PL emission spectra using $\bar{x}(\lambda), \bar{y}(\lambda)$ and $\bar{z}(\lambda)$ color matching functions defined in the CIE 1931. For a specified power spectral density P(λ), the degree of stimulation required to match the color of P(λ) is given by three equations:

$$X = \int_{\lambda} \bar{x}(\lambda)P(\lambda)d\lambda$$

$$Y = \int_{\lambda} \bar{y}(\lambda)P(\lambda)d\lambda$$

$$Z = \int_{\lambda} \bar{z}(\lambda)P(\lambda)d\lambda$$

where *X, Y*, and *Z* are the tristimulus values. The tristimulus value provides stimulation (i.e. power) value for each of three primary (red, green, blue) colors to match the color of P(λ).

The tristimulus values specifying the color is stored in the ratio of the primary colors and not in the specific amounts of each individual primary color, the number of dimensions used to match the color of P(λ). This was done for the CIE 1931 *XYZ* space, and the resultant CIE 1931 *x-y* chromatic diagram is the most commonly used tool, to describe color, in spectroscopy today. From *(X, Y, Z)*, the *(x, y)* chromaticity coordinates are calculated as:

$$x = \frac{X}{X + Y + Z}$$

$$y = \frac{Y}{X + Y + Z}$$

Further, the quality of white light is evaluated from the chromaticity coordinates using McCamy's relation,[26] by first evaluating ratio between inverse slope line and chromaticity epicentre as:

$$n = \frac{(x - x_e)}{(y - y_e)}$$

where x_e= 0.3320 and y_e =0.1858. Then the Correlated Color Temperature (CCT) was evaluated as:

$$CCT = -449n^3 + 3525n^2 - 6823.3n + 5520.33$$

The color purity or color saturation of a light source is the distance in the chromaticity diagram between the *(x, y)* color-coordinate point of the test source and the coordinate of the equal-energy point divided by the distance between the equal-energy point and the dominant wavelength point. The color purity is thus given by:

Journal Name

$$\text{Color purity} = \frac{\sqrt{(x-x_{ee})^2+(y-y_{ee})^2}}{\sqrt{(x_d-x_{ee})^2+(y_d-y_{ee})^2}}$$

where, (x, y), (x_{ee}, y_{ee}) and (x_d, y_d) represent the chromaticity coordinates of the light source under test, equal-energy reference illuminant and dominant-wavelength point, respectively.[27]

4. Results and discussion

4.1 Structural and morphological analysis

The crystal structure of $BaNb_2O_6$ compound was reported for the first time by Sirotinkin *et al*. in 1990, and has orthorhombic [space group $C222_1$ (20)] structure with cell parameters a = 7.880 Å, b = 12.215 Å, c =10.292 Å and Z = 8.[28] The phase purity of the as-prepared phosphors was characterized using XRD. Fig. 1 illustrates the XRD patterns of undoped and Dy^{3+} ions doped $BaNb_2O_6$ phosphors that are in agreement with the PDF-4+(ICDD) standard card no. 04-012-8861. It was found that there is no change in peak positions among all XRD patterns, which indicate pure phase formation for undoped and doped $BaNb_2O_6$ phosphors with respect to their corresponding (hkl) planes. This fact could be due to large ionic radius of Ba^{2+} (1.24 Å) than Dy^{3+}(0.95 Å) and Dy^{3+} ions may occupy Ba^{2+} sites when they enter into $BaNb_2O_6$ host lattice. Hence, no additional peaks were found up to 2 mol% doping of Dy_2O_3, which means that Dy^{3+} ions were successfully substituted for Ba^{2+} ions without changing crystal structure of the host lattice.

The average crystallite size (D) and strain (ε) of the samples were calculated using most reliable Williamson–Hall (W-H) equation[29, 30] $[\beta\ Cos\ \theta = \left(\frac{K\lambda}{D}\right) + 4\varepsilon\ Sin\theta]$, where K = shape factor (0.94), D is average crystallite size, λ is wavelength of CuKα radiation, θ is Bragg's diffraction angle of the planes and β is the corrected full width at half maximum (FWHM). The average crystallite size of $Ba_{(1-x)}Nb_2O_6$: xDy^{3+} (x = 0.0, 0.1, 0.5, 1.0 and 2.0 mol%) samples was found to be in the range 44 and 55 nm. The strain present in lattice was calculated and the values for x = 0.0, 0.1, 0.5, 1.0 and 2.0 mol% Dy^{3+} ions doped $BaNb_2O_6$ sintered at 1200^oC were found to be 0.081, 0.114, 0.113, 0.061 and 0.091, respectively. Further the average crystallite size calculated by Debye - Scherer's formula[31] $[D = K\lambda/\beta Cos\theta]$ was found to be in the range 40 and 89 nm and is in good agreement with the calculations performed using W-H method.[32] The Rietveld refinement of undoped $BaNb_2O_6$ was carried out using FullProf software shown in Fig. 2 (a) and the resulting parameters are summarized in Table 1. The results indicate a good agreement between the observed and calculated diffraction patterns of orthorhombic phase [space group $C222_1$ (20)] without any anonymous peak.[33] The unit cell parameters were determined and are found to be a =7.8707 Å , b = 12.2096 Å, c =10.2881 Å and cell volume (V) = 988.680 $Å^3$, which are close to those reported by Sirotinkin *et al* [27]. The refinement finally converging to goodness-of-fit parameter (χ^2) = 4.2%, R_{wp} = 31.0% and R_p = 25.6%. Fig. 2(b) shows the orthorhombic structure of $BaNb_2O_6$ lattice projected onto b-c plane.

Fig. 3(a) & (b) represents SEM micrograph of 0.5 mol% Dy^{3+} ions doped $BaNb_2O_6$ phosphor. The micrograph reveals inhomogeneous and uneven dense morphology in micrometer range. The typical crystalline particle size is the range of 4-6 micrometer in dimension. It is obvious that, micrometer sized

crystalline powder would be very much suitable to produce an efficient white light for solid-state lighting applications.[34]

4.2 Photoluminescence studies

The Fig. 4 illustrates the PLE spectrum of the $Ba_{(1-x)}Nb_2O_6$:xDy^{3+} (x=0.5 mol%) phosphor by monitoring the emission wavelength at 574 nm. The PLE spectrum consists of seven sharp peaks due to intra 4f-4f transitions located at 326, 349, 364, 386, 427, 454 and 474 nm, which are attributed from ground state $^6H_{15/2}$ to the different excited states $(^6P_{3/2},^4M_{17/2})$, $^6P_{7/2}$, $(^4I_{11/2},^6P_{5/2})$, $(^4F_{7/2},^4I_{13/2})$, $^4G_{11/2}$, $^4I_{15/2}$ and $^4F_{9/2}$, respectively.[35, 36]

Fig. 5(a) shows the PL emission spectra of $Ba_{(1-x)}Nb_2O_6$:xDy^{3+} (x= 0.01, 0.1, 0.5, 1.0, 1.5, 2.0, 2.5 mol%) phosphors with different doping concentration of Dy^{3+} ions at 386 nm excitation wavelength. Emission spectra exhibit two intense peaks at 482 and 574 nm and a very weak peak at 664 nm corresponding to the $^4F_{9/2} \rightarrow^6H_{15/2}$, $^4F_{9/2} \rightarrow^6H_{13/2}$, and $^4F_{9/2} \rightarrow^6H_{11/2}$ transitions, respectively.[35] The $^4F_{9/2} \rightarrow^6H_{15/2}$ transition belongs to the magnetic dipole allowed and its intensity does not depend on crystal field of the host.[38] On the other hand, the intensity of the hypersensitive transitions (ΔL=2; ΔJ=2) correspond to $^4F_{9/2} \rightarrow^6H_{13/2}$ belongs to a forced electric dipole transition, which is allowed in case that Dy^{3+} ions are located at the local sites with non-inversion center symmetry.[38-40] In Dy^{3+} doped $BaNb_2O_6$ phosphor, the intensity of yellow emission $(^4F_{9/2} \rightarrow^6H_{13/2})$ is stronger than blue $(^4F_{9/2} \rightarrow^6H_{15/2})$ that confirms the location of the active ions (Dy^{3+}) in low symmetry environment without the inversion centre in the host. As the radius of Dy^{3+} ions is less than Ba^{2+}, Dy^{3+} ions can easily enter into Ba^{2+} sites having low symmetry. This is in good agreement with the results obtained from XRD analysis.[41] Moreover, the emission spectra of the sample $Ba_{(1-x)}Nb_2O_6$:xDy^{3+} measured at 349, 364, 386 and 399 nm excitations as shown in inset of Fig 5(b). The similar profile of emission lines has been observed with different intensities for each excitation. The emission intensity at 386 nm excitation is considered as optimum as its intensity is higher than the emission intensity observed for other excitation wavelengths. This may be due to relatively higher absorption at that wavelength.

The branching ratio (β) is a critical parameter to calculate the relative intensities of emission lines originating from $^4F_{9/2}$ excited state. The branching ratios for yellow and blue transitions originating from $^4F_{9/2}$ were calculated by taking the integrals under respective emission bands. For all Dy^{3+} ion concentrations, the sum of the branching ratios for the corresponding emission bands $^4F_{9/2} \rightarrow^6H_{15/2}$ and $^4F_{9/2} \rightarrow^6H_{13/2}$ were found to be unity $(\beta_{482} + \beta_{574})$ suggesting that both the transitions have wide possibility of attaining stimulated emission with higher efficiency.[42] Moreover, it could be noticed that the emission band $^4F_{9/2} \rightarrow ^6H_{15/2}$ is broadened and also observed that this transition splits into a maximum number of J + ½ Stark components in the blue emission region (450-500 nm), where J is the total angular momentum of electrons.[43, 44]

In Fig. 5(a), the emission intensity increases initially with an increase in concentration of Dy^{3+} ions and reaches to a maximum at x= 0.5 mol% and then gradually decreases beyond 0.5 mol% due to concentration quenching phenomenon. As the doping concentration of Dy^{3+} ions increases, the distance between luminescent centres decreases that increases the possibility of non-radiative energy transfer.[45] The concentration quenching phenomenon resulted mainly by the non-radiative energy transfer among Dy^{3+} ions. In the present system, energy transfer

mechanism from one Dy^{3+} ions to another depends on critical distance between Dy^{3+}-Dy^{3+} ions. Hence, the critical distance (R_c) between the adjacent Dy^{3+} ions could be necessary to calculate. According to Blasse[46, 47, 45] the critical distance could be expressed as:

$$Rc \approx 2\left[\frac{3V}{4\pi X_c N}\right]^{\frac{1}{3}}$$

where, V is the volume of unit cell, X_c is the critical/optimised concentration (mole) of the activator ions and N is the number of cations per unit cell. By analyzing the experimental data, the values are found to be V=988.68 $Å^3$, N =8 and X_c = 0.005. The calculated critical energy transfer distance is 36 Å for the current system. Van Uitert[48] has pointed out energy transfer generally associated with exchange interaction, radiation re-absorption, or multipolar interactions. The exchange interaction is usually accountable for the energy transfer for the forbidden transition and the critical distance of about 5 Å.[47] Since, the distance between adjacent Dy^{3+} ions is larger than 5 Å, as a result the exchange interaction becomes ineffective and multipolar interaction will become important in this case. According to Dexter's theory, when the doping amount of the activator is large enough, the luminescence intensity I and the mole fraction of activator ions x could be related as follows[49, 50]:

$$log(I/x) = -\frac{Q}{3}log\, x + A$$

where, A is a constant and Q represents interaction type between rare-earth ions. If Q=6, 8 and 10, the interaction may be corresponding to the electric dipole-dipole (d-d), dipole-quadrupole (d-q) and quadrupole-quadrupole (q-q) interactions, respectively.[51] Depending on the emission spectra of $Ba_{(1-x)}Nb_2O_6$:xDy^{3+} excited at 386 nm, the correlation between $log(I/x)$ and $log(x)$ is shown in Fig. 6. The calculated value of Q is 4.95, which is close to 6 discloses that the concentration quenching mechanism in the $BaNb_2O_6$:Dy^{3+} phosphor occurs due to electric dipole-dipole (d-d) interaction.[52, 45]

The radiative emission process explained as that the radiation excites the Dy^{3+} ions to the higher excited levels and then quickly relaxed to the $^4F_{9/2}$ level by non-radiative and radiative transfer from $^4F_{9/2}$ excited level as shown in schematic energy level diagram in Fig. 7. The upward and downward arrows indicate in this figure represent excitation and emission, respectively. The possible non-radiative channels explained in Fig. 7 could be : (i) the possible resonant energy transfer (RET): ($^4F_{9/2}$+$^6H_{15/2}$ → $^6H_{15/2}$+$^4F_{9/2}$) by considering the energy match rule, and (ii) cross relaxation channels (CRC1, CRC2 and CRC3) among Dy^{3+} ions are responsible for de-population of $^4F_{9/2}$ energy level by non-radiative such as ($^4F_{9/2}$+$^6H_{15/2}$→$^6F_{11/2}$, $^6H_{9/2}$+$^6F_{5/2}$), ($^4F_{9/2}$+$^6H_{15/2}$→$^6F_{9/2}$, $^6H_{7/2}$+$^6F_{5/2}$) and ($^4F_{9/2}$+$^6H_{15/2}$→ $^6F_{1/2}$+$^6F_{11/2}$, $^6H_{9/2}$) for as prepared phosphors.[53, 41, 45]

Further, the luminescence intensity ratio of yellow to blue (Y/B) is essential for white-light emission. The calculated (Y/B) ratio for the optimized excitation wavelength of 386 nm was found to be close to unity for all doping concentrations. There has been slight variation in the value of the ratio near to unity for other three excitations wavelengths namely, 349, 364 and 399 nm, which confirms excellent stability of the color coordinates against different excitations and concentrations. The intensity ratio being almost constant was attributed to the local environment around

Dy^{3+} ions and is invariant with the varying concentration of Dy^{3+} ions.[39]

4.3 CIE chromaticity coordinates

The Fig. 8 shows the CIE chromaticity coordinates for the optimised sample calculated from the emission spectra measured under different excitations. The CIE chromaticity coordinates for optimized phosphor were found to be (0.312, 0.343), (0.319, 0.364), (0.322, 0.339) and (0.312, 0.342) for corresponding excitations 349, 364, 386, 399 nm, respectively and are indicated in Fig. 8. An excellent white-light chromaticity coordinates (0.322, 0.339) were observed for 386 nm excitation and is very close to the standard equal energy white-light point (0.333, 0.333). The CIE chromaticity coordinates under optimized excitation (λ_{ex}=386 nm) for different Dy^{3+} ions concentration is given Table.2. It is interesting to note that the optimized $Ba_{(1-x)}Nb_2O_6$:xDy^{3+} (x=0.5 mol%) phosphor sample exhibited superior white luminescence coordinates compared to different Dy^{3+} doped phosphor hosts such as $CaMoO4$:Dy^{3+} (0.28, 0.27)[41], $Sr_3Gd(PO_4)_3$:Dy^{3+} (0.25, 0.29)[45], YPO_4:Dy^{3+} (0.36, 0.42)[22] and found to be extremely close to commercial pc-LED (Blue LED+YAG:Ce^{3+}) and National Television System Committee (NTSC) white-light emission having (0.32, 0.32) and (0.310, 0.316), respectively.

The calculated CCT values for Dy^{3+} ions doped $BaNb_2O_6$ phosphors were found to vary between 5689-6373 K and falls in cool-white region. The calculated CCT was 5907 K for optimized concentration (x=0.5 mol%) of $BaNb_2O_6$:Dy^{3+} phosphor, which represents cool-white emission and is very close to "ideal white" region of the chromaticity diagram. The higher value of CCT indicates better visual acuity and greater brightness perception as compared to lower values.[54] The CCT values lie in the cool white-light region signifying the possibility of the phosphor for application in w-LEDs for outdoor illumination.

Using the chromaticity coordinates given in Fig. 8 for optimized concentration of as-prepared phosphor, the color purity was calculated and found to be around 7.89×10^{-2}, 5.39×10^{-2}, 5.39×10^{-2} and 7.89×10^{-2} corresponding to 349, 364, 386, 399 nm excitations wavelengths, respectively. The low value of the color purity indicates the purity for white-light emission.[53, 27] The above-mentioned results indicate that the as-prepared phosphor can be considered as a potential candidate for fabrication w-LEDs based on NUV chips as excitation source.

4.4 Luminescence decay curve analysis

The room-temperature luminescence decay curve has been plotted for $Ba_{(1-x)}Nb_2O_6$:xDy^{3+} (x=0.5 mol %) phosphor and is shown in Fig. 9. It represents the decay curve of $^4F_{9/2}$→ $^6H_{13/2}$ emission for phosphor when excited under 386 nm wavelength. To understand the behaviour of luminescent decay, the decay curve was fitted with different equations and the best fit was observed for bi-exponential equation[55, 56]:

$$I = A_1\, e^{-t/\tau_1} + A_2\, e^{-t/\tau_2}$$

where, I is the luminescence intensity; t is time; τ_1 and τ_2 are the decay time for the exponential component and A_1 and A_2 are the fitting parameter constants, respectively. Thus, the average lifetime in case of bi-exponential fitting can be determined by using equation:[41]

$$\tau_{avg} = \frac{A_1\tau_1^2 + A_2\tau_2^2}{A_1\tau_1 + A_2\tau_2}$$

The fluorescent lifetime τ_{avg} for $^4F_{9/2}$ level for optimized phosphor sample was found to be ~146.07 µs. Generally, the PL decay curves can be influenced by energy transfer between Dy^{3+} ions. If there is no interaction between the rare-earth ions, the decay curves are usually fitted to a single exponential function. The bi-exponential fitting behaviour shows the possibility of interaction between Dy^{3+} ions in $BaNb_2O_6$ lattice as discussed in the previous sections.

5. Conclusions

Single-phase $BaNb_2O_6$:Dy^{3+} white-light emitting phosphors were successfully synthesized using solid-state reaction method. The crystallinity and pure phase of the as-prepared phosphors were examined by XRD and Rietveld refinement studies. All the prepared samples exhibited single-phase with orthorhombic structure. The excitation spectra indicate that the phosphors could be effectively excited by NUV LED chips having excitation wavelength of 386 nm. In order to determine the optimized doping concentration of $BaNb_2O_6$:Dy^{3+} phosphors, the luminescent measurements were carried out. 0.5 mol% of Dy^{3+} has been found to be the optimum doping concentration under different excitation wavelengths. The blue (482 nm) and yellow (574 nm) emission bands corresponding to $^4F_{9/2} \rightarrow {}^6H_J$ (J= 15/2, 13/2) transitions and the value of Y/B ratio close to unity has been successfully achieved. The combination of these emission bands emit white-light and the CIE chromaticity coordinates for the optimized phosphor is (x=0.322, y= 0.339) with CCT value of 5907 K, which is close to the standard white-lamp calorimetric point in cool white region. All the above-mentioned results indicate that the Dy^{3+} ions doped $BaNb_2O_6$ phosphor could be used as a practical potential luminescent material for NUV based w-LED applications.

Acknowledgements

References

1. M. Zhang, Y. Liang, R. Tang, D. Yu, M. Tong, Q. Wang, Y. Zhu, X. Wu, G. Li, *RSC Adv.*, 2014, **4**, 40626-40637.
2. H. Qian, J. Zhang, L. Yin, *RSC Adv.*, 2013, **3**, 9029-9034.
3. S. H. Park, K. H. Lee, S. Unithrattil, H. S. Yoon, H. G. Jang, W. B. Im, *J. Phys. Chem. C*, 2012, **116**, 26850-26856.
4. Y. Uchida, T. Taguchi, *Opt. Eng.*, 2005, **44** (12), 124003-9.
5. H. S. Jang, W. Im Bin, D. C. Lee, D.Y. Jeon, S. S. Kim, *J. Lumin*., 2007, **126** (2), 371–377.
6. S. Nakamura, S. Pearton, G. Fasol. *The Blue Laser Diode- the complete story*, 1997, Springer- Verlag Berlin Heidelberg GmbH, pp. 230-231.
7. J. K. Sheu, S. J. Chang, C. H. Kuo, Y. K. Su, L. W. Wu, Y. C. Lin, W. C. Lai, J. M. Tsai, G. C. Chi, R. K. Wu, *IEEE Photon. Technol. Lett.*, 2003, **15**, 18-20.
8. K. Li, X. Liu, Y. Zhang, X. Li, H. Lian, J. Lin, *Inorg. Chem.*, 2015, **54**, 323-333.
9. T. Jia, Z. Ci, Q. Wu, G. Zhu, C. Wang, Y. Wang, *ECS J. Solid State Sci. Technol.*, 2015, **4**(5), R78-82.
10. J. McKittrick, L. E. Shea-Rohwer, *J. Am. Ceram. Soc.*, 2014, **97**, 1-26.
11. M. Shang, C. Li, J. Li, *Chem. Soc. Rev.*, 2014, **43**, 1372-1386.
12. H. Zhu,Z. Zheng, X. Gao, Y. Huang, Z. Yan, J. Zou, H. Yin, Q. Zou, S. H. Kable, J. Zhao, Y. Xi, W. N. Martens, R. L. Frost, *J. Am. Chem. Soc.*, 2006, **128**, 2373-2384.
13. P. W. C. Sarvezuk, E. J. Kinast, C. V. Colin, M. A. Gusmao, J. B. M. da Cunha, O. Isnard, *J. Appl. Phys.*, 2011, **109**, 07E160-3.
14. D. V. D. Voort, J. M. E. De Rijk, G. Blasse, *Phys. Stat. Sol.*, 1993, **135**, 621-626.
15. F. Huang, Q. Zhou, C. Ma, L. Li, X. Huang, F. Li, Q. Cui, D. Xu, W. Wang, T. Cui, G. Zou. *RSC Adv.*, 2013, **3**, 13210-13213.
16. S. Lei, D. Guo, C. Wang, D. Cheng, X. Gao, S. Zeng, Y. Xiao, B. Cheng, *Cryst. Engg. Comm.*, 2014, **16**, 7949-7955.
17. R. C. Pullar, J. D. Breeze, N. M. Alford, *J. Am. Ceram. Soc.*, 2005, **88** (9), 2466-2471.
18. A. K. Vishwakarma, K. Jha, M. Jayasimhadri, A. S. Rao, K. Jang, B. Sivaiah, D. Haranath, *J. Alloys Compd.*, 2015, **622**, 97-101.
19. Y. Zhou, Z. Qui, M. Lu, Q. Ma, A. Zhang, G. Zhou, H. Zhang, Z. Yang, *J. Phys. Chem. C*, 2007, **111**, 10190-10193.
20. M. K. Ekmekci, M. Erdem, A. S. Basak, *Dalton Trans.,* 2015, **44**, 5379-5385.
21. M. K. Ekmekci, M. Erdem, A. Mergen, G. Ozen, B.D. Bartolo, *J. Alloys. Compd.,* 2014, **591**, 230-233.
22. **A.**K. Parchur, A. I. Prasad, S. B. Rai and R. S. Ningthoujam, *Dalton Trans.*, 2012, **41**, 13810-13814.
23. M. Jayasimhadri, B. V.Ratnam, K. Jang, H. S. Lee, *Int. J. Appl. Ceram. Technol.*, 2011, **8**, 709-717.
24. K. Mishra, S. K. Singh, A. K. Singh, S. B. Rai, *Mater. Res. Bull.*, 2012, **47**, 1339-1344.
25. S. Dutta, S. Som, S. K. Sharma, *Dalton Trans.*, 2013, **42**, 9654-9661.
26. C. S. McCamy, Color Res. Appl., 1992, **17**, 142-144.
27. E. F. Schubert, *Light emitting Diodes 2ⁿᵈ Ed.*, Cambridge University Press Newyork, 2006, pp. 292.
28. V. P. Sirotinkin, S. P. Sirotinkin, *Russ. J. Inorg. Chem.*, 1990, **35**, 1246-1248.
29. B. D. Cullity, *Elements of X-Ray Diffraction*, Addison-Wesley, Massachusetts, 1956, pp. 312.
30. S. Bathula, B. Gahtori, M. Jayasimhadri, S. K. Tripathy, K. Tyagi, A. K. Srivastava, A. Dhar, *Appl. Phys. Lett.,* 2014, **105**, 061902-4.
31. B. P. Singh, A. K. Parchur, R. K. Singh, A. A. Ansari, P.Singh, S. B. Rai, *Phys. Chem. Chem. Phys.*, 2013, **15**, 3480-3489.
32. A. K. Parchur, R. S. Ningthoujam, *Dalton Trans.*, 2011, **40**, 7590-7594.
33. H. M. Rietveld, *J. Appl. Cryst.*, 1968, **2**, 65-71.
34. Y. Zhou, Q. Ma, M. Lu, Z. Qiu, A. Zhang, *J. Phys. Chem. C.*, 2008, **112**, 199901-19907.
35. D. L. Monika, H. Nagabhushana, R. H. Krishna, B. M Nagabhushana, S. C. Sharma, T. Thomas, *RSC Adv.*, 2014, **4**, 38655-38662.
36. E. Pavitra, G. S. R. Raju, W. Park, J. S. Yu, *New J. Chem.*, 2014, **38**, 163-169.
37. B. V. Ratnam, M. Jayasimhadri, K. Jang, H. S. Lee, *J. Am. Ceram. Soc.*, 2010, **93**, 3857-3861.
38. Z. Ci, Q. Sun, S. Qin, M. Sun, X. Jiang, X. Zhang, Y. Wang, *Phys. Chem. Chem. Phys.*, 2014, **16**, 11597-11602.
39. Q. Su, Z. Pei, L. Chi, H. Zhang, Z. Zhang, F. Zou, *J. Alloys Compd.*, 1993, **192**, 25-27.
40. J. L. Fry, H. H. Caspers, H. E. Rast, S. A. Miller, *J. Chem. Phys.*, 1968, **48**, 2342-2348.

41. S. Dutta, S. Som, S. K. Sharma, *Dalton Trans.*, 2013, **42**, 9654-9661.
42. M. Jayasimhadri, K. Jang, H. S. Lee, B. Chen, S. S. Yi, J. H. Jeong, *J. Appl. Phys.*, 2009, **106**, 013105-4.
43. G. H. Dieke, S. Singh, *J. Opt. Soc. Am.*, 1956, **46** (7), 495-499.
44. B. Liu, C. Shi, *Appl. Phys. Lett.*, 2005, **86**, 191111-3.
45. Q. Liu, Y. Liu, Z. Yang, Y Han, X. Li, G. Fu, *J. Alloys Compd.*, 2012, **515**,16-19.
46. G. Blasse, *Philips Res. Rep.*, 1969, **24** (2), 131-144.
47. Q. Xu, J. Sun, D. Cui, Q. Di, J. Zeng, *J. Lumin.*, 2015, **158**, 301-305.
48. L. G. Van Uitert, *J. Electrochem. Soc.* 1967, **114**, 1048-1053.
49. D. L. Dexter, *J. Chem. Phys.*, 1953, **21**, 836-850.
50. D. L. Dexter, J. H. Schulman, *J. Chem. Phys.*, 1954, **22**, 1063-1070.
51. H. Li, R. Zhao, Y. Jia, W. Sun, J. Fu, L. Jiang, Su. Zhang, R. Pang, C. Li, *Appl. Mater. Interfaces,* 2014, **6**, 3163-3169.
52. L. Zhang, H. Zhong, X. Li, L. Cheng, Li. Yao, J. Sun, J. Zhang, R. Hua, B. Chen, *Physica B*, 2012, **407**, 68-72.
53. J. S. Kumar, K. Pavani, A. M. Babu, N. K. Giri, S. B. Rai, L. R. Moorthy, *J. Lumin.*, 2010, **130**, 1916-1923.
54. M. R. N. Soares, M. J. Soares, A. J. S. Fernandes, L. Rino, F. M. Costa, T. Monteiro, *J. Mater. Chem.*, 2011, **21**, 15262-15265.
55. B. C. Jamalaiah, J. S. Kumar, A. M. Babu, L R. Moorthy, K. Jang, H. S. Lee, M. Jayasimhadri, J. H. Jeong, H. Choi, *J. Lumin.*, 2009, **129**, 1023-1028.
56. M. Jayasimhadri, L. R. Moorthy, R. V. S. S. N. Ravikumar, *Opt. Mater.*, 2007, **29**, 1321-1326.

Tables

**Table 1.** Calculated crystallographic data of $BaNb_2O_6$ by Rietveld refinement method.

Formula	$BaNb_2O_6$
Radiation	Cu Kα
2 θ (°)	20-60
Symmetry	Orthorhombic
Space group	$C222_1$ (20)
a(Å)	7.8707
b(Å)	12.2096
c(Å)	10.2881
α (°)	90
β (°)	90
γ (°)	90
Z	8
R_p	25.6
R_{wp}	31.0
X^2	4.2
V($Å^3$)	988.680
Density (mg/m^3)	5.62

Table 2. Y/B ratio, CIE chromaticity coordinates and CCT for $BaNb_2O_6$:Dy^{3+} phosphors at various doping concentrations.
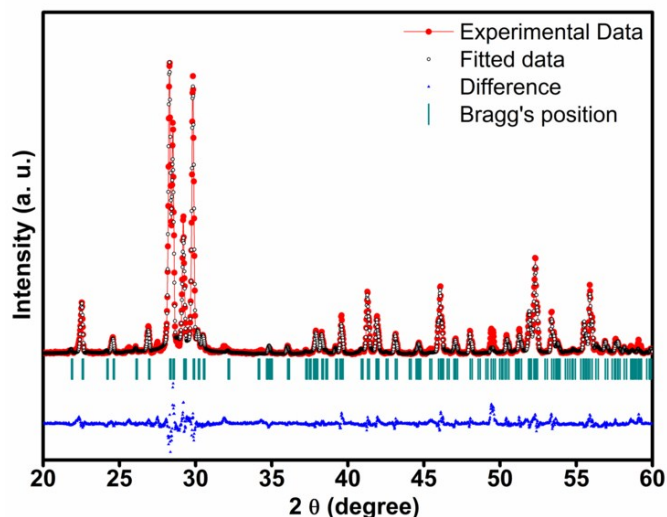
λ_{ex}=386 nm			
X (Dy^{3+} concentration in mol%)	Y/B ratio	(x, y)	CCT (K)
0.01	1.11	(0.329, 0.339)	5689
0.10	1.06	(0.322, 0.338)	6000
0.50	1.01	(0.322, 0.339)	5907
1.00	1.05	(0.314, 0.341)	6373
1.50	1.06	(0.320, 0.340)	6056
2.00	1.11	(0.331, 0.332)	5623
2.50	1.07	(0.312, 0.319)	6652

Figures
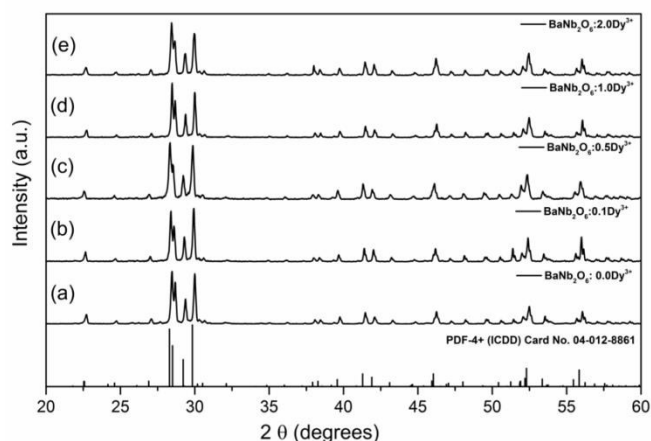
Fig. 1: Powder XRD patterns of $Ba_{(1-x)}Nb_2O_6$:xDy^{3+} (x=0.0, 0.1, 0.5, 1.0, 2.0 mol%) phosphors.

Fig. 2(a): Experimental, calculated and difference in X-ray diffraction pattern of $BaNb_2O_6$ powder.
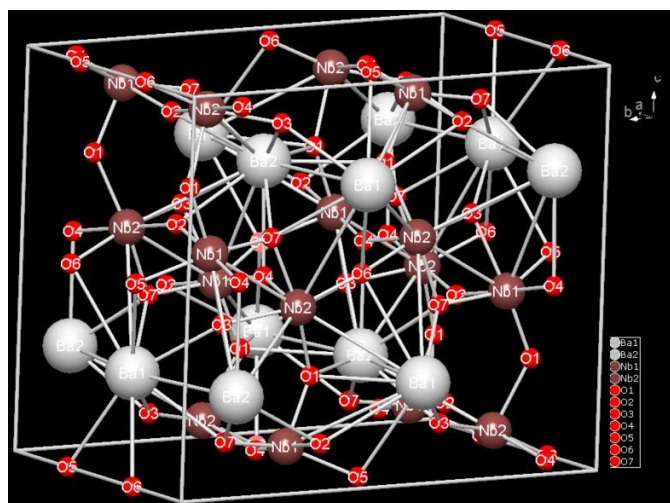
Dalton Transactions Accepted Manuscript

Fig. 2(b): Crystal structure of $BaNb_2O_6$ in b-c plane.
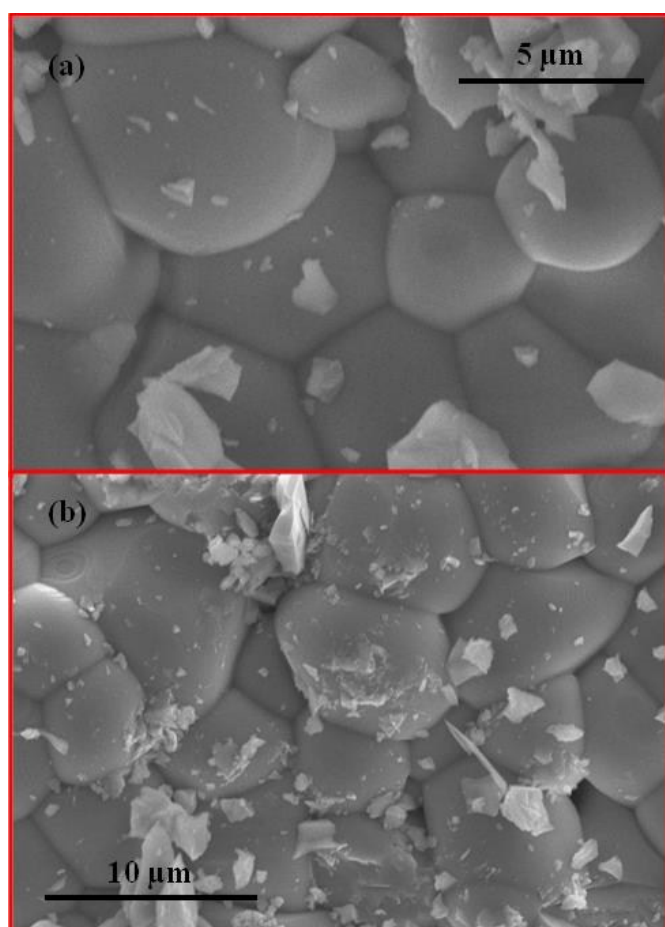
Fig. 3: (a & b). SEM micrographs of $Ba_{(1-x)}Nb_2O_6:xDy^{3+}$ (x=0.5 mol%) phosphor sintered at 1200^oC.
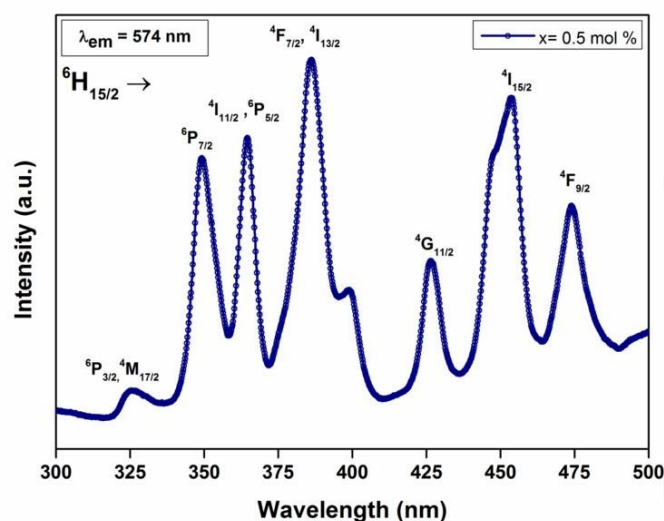
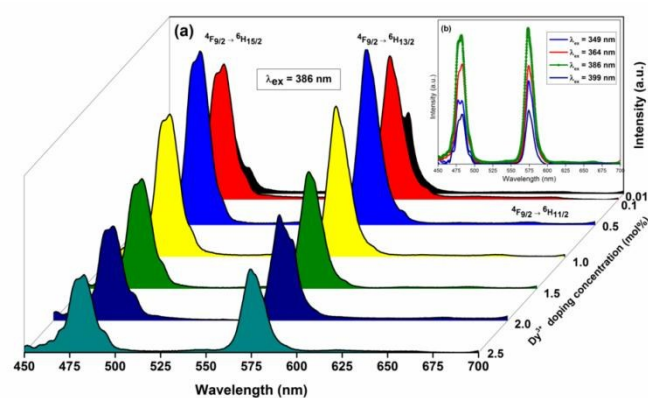**Fig. 4:** Photoluminescence excitation spectra (λ_{em}=574 nm) of $Ba_{(1-x)}Nb_2O_6:xDy^{3+}$ (x=0.5 mol%) phosphor.

Fig. 5: (a) Emission spectra (λ_{ex}=386 nm) of $BaNb_2O_6:Dy^{3+}$ phosphor at different mol% concentration of Dy^{3+} ions. **(b)** emission spectra of $Ba_{(1-x)}Nb_2O_6:xDy^{3+}$ (x=0.5 mol%) phosphor at different excitations (λ_{ex}=349, 364, 386, 399 nm) (in inset).
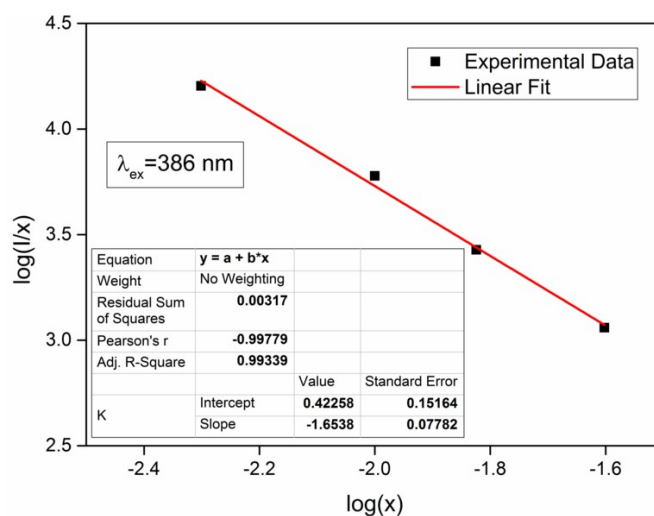

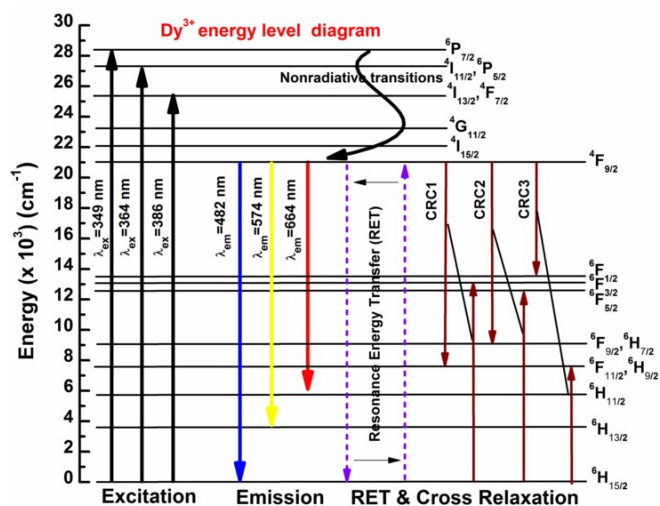**Fig. 6:** Relationship of log(I/x) with log(x) in $BaNb_2O_6:Dy^{3+}$ phosphor under 386 nm excitation

Fig. 7: Partial energy level diagram illustrating excitation, emission and energy transfer mechanisms of Dy^{3+} ions in $BaNb_2O_6$ phosphors.

Fig. 8: CIE chromaticity diagram for Dy^{3+} ions doped $BaNb_2O_6$ phosphor.

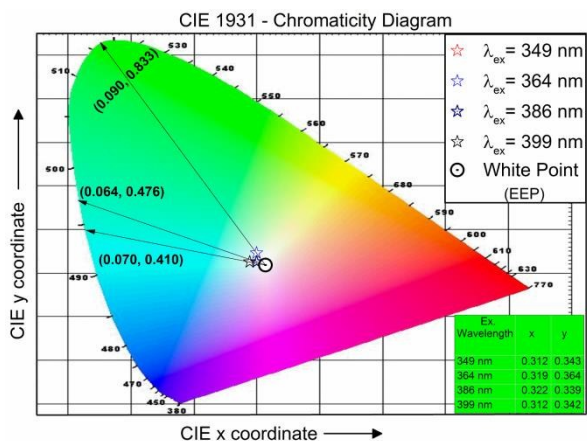**Fig. 9:** Luminescence decay curve (λ_{em}=574 nm) of $Ba_{(1-x)}Nb_2O_6$:xDy^{3+} (x=0.5 mol%) phosphor under 386 nm excitation.